Stable, π-conjugated radical anions of boron-nitrogen dihydroindeno[1,2-b]fluorenes

Tony Nguyen[1], Tyler J. Hannah[1], Warren E. Piers[1]* and Benjamin S. Gelfand[1]

[1]University of Calgary, Department of Chemistry, 2500 University Drive N.W., Calgary, Alberta, Canada, T2N 1N4

Corresponding Author: Warren E. Piers (email: wpiers@ucalgary.ca)

Table of Contents Graphic.

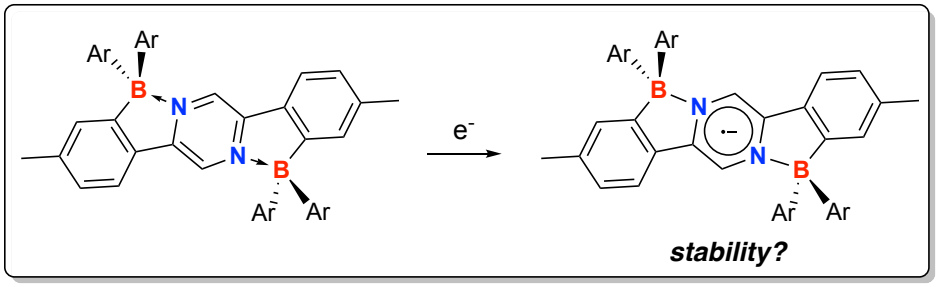

Synopsis:

Radical anions of two new boron-nitrogen dihydroindeno[1,2-b]fluorenes are reported and fully characterized. The SOMO is localized in the planar core of the molecule, preventing dimerization. Under inert conditions, the radical anions are indefinitely stable but degrade under ambient atmosphere.

Abstract

We have recently reported the synthesis and application of boron-nitrogen dihydroindeno[1,2-b]fluorene derivatives as acceptors in organic photovoltaic (OPV) devices. Their modest observed efficiencies may be related to the properties of their reduced congeners. In this work, we report two new members of this family of compounds prepared via the electrophilic borylation of 2,5-di-*p*-tolylpyrazine followed by an arylation of the boron centre with $ZnAr_2$ reagents. Two derivatives, **1** (Ar = 2,4,6-$F_3C_6H_2$) and **2** (Ar = C_6F_5) were synthesized, and their radical anions, $\mathbf{1}^{\bullet-}$ and $\mathbf{2}^{\bullet-}$, were formed via chemical reductions with $CoCp^*_2$ and $CoCp_2$, respectively. Through comparison of structural parameters, as well as spectroscopic and computational data, the unpaired electron in the radical anions is localized in the planar core of the molecule, and dimerization is disfavored as a result. However, unlike the neutral starting materials, $\mathbf{1}^{\bullet-}$ and $\mathbf{2}^{\bullet-}$ are reactive towards ambient atmosphere. These observations suggest that the reduced compounds are stable towards intrinsic degradation pathways but subject to extrinsic degradation in device operation.

Key words: radical anions, boron, heterocycles

Introduction

Polycyclic aromatic molecules and polymers are well studied materials for use in organic photovoltaic (OPV) or light emitting (OLED) devices. A subset of these materials is comprised of molecules and materials having one or more of the C-C units in the framework substituted with the isosteric and isoelectronic B-N moiety,[1-5] which has been shown to impart unique reactivity,[6-8] photophysical,[1, 9, 10] and redox properties[11-13] compared to their carbonaceous counterparts. The B-N functionality introduces a bond polarization that can impact crystal packing[14, 15] and generally

lowers the reduction potential of the materials. The modern era of "BN for CC"[1, 2, 14] organic materials has produced a large variety of conjugated structures[3, 16-18] and electrophilic borylation, originally introduced by the pioneering work of Dewar,[19] is one of the primary tools for assembling such frameworks.[20]

The comparably low reduction potentials of BN heteroaromatics vs their CC congeners suggests they are viable n-type acceptor materials for use in OPV bulk heterojunction type photovoltaic cells.[21, 22] A challenge for these types of acceptors is the rate at which they undergo extrinsic or intrinsic degradation when operating in a device, which lowers their utility over medium to longer time periods.[23] Extrinsic degradation is related to their instability towards oxygen and/or water when reduced and can to some extent be dealt with by using device engineering to exclude water and oxygen from permeating the device. Intrinsic degradation refers to processes of radical dimerization and/or crosslinking[24, 25] that occurs when reduced n-type acceptors are produced during the operation of the device. To understand these processes and mitigate against them, it is important to investigate the properties of the radical anions formed upon acceptance of an electron in new families of potential BN materials for use in these applications.

While there are several examples of boron-based radical anions,[26-32] those of BN containing materials are somewhat more rare.[33] The $(BN)_2$ triphenylenes we reported in 2003[11] are readily reduced by one electron to persistent radical anions that could be fully characterized[12] (**I**, Chart 1). The BNB-doped phenalenyl complexes of Wagner *et al.* (**II**) require somewhat harsher reducing agents but nonetheless form detectable radical anions that scavenge hydrogen atoms effectively.[34] Both the Otten[35] and Gilroy[36] groups have explored the chemistry of the radical anions of diaryl and dialkynyl borane complexes of formazanate ligands (**III**). Most germane to the work reported

here, Pammer *et al.* have reported radical anions of the partially saturated BN ladder heterocycles **IV**[37] in which the SOMO is mostly localized on the core pyrazine moiety of the framework. We have recently reported fully conjugated BN dihydroindeno[1,2-b]fluorenes and evaluated their performance as acceptors in OPVs.[22] Since the observed efficiency of the resulting devices was relatively low, we decided to examine the redox properties of a derivative of these compounds in more detail. Herein we report the synthesis of two new compounds (**V**, Chart 1) in this family and describe their reduction chemistry, including the full characterization of the radical anions that result from one electron reduction.

Chart 1.

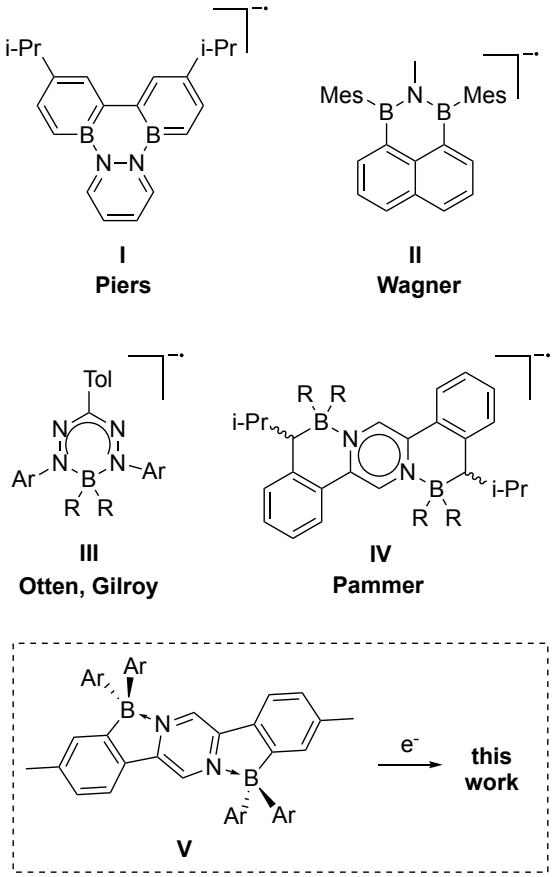

Results and discussion

Synthesis and Structure. Previously studied examples of heterocycles **V** incorporated *t*-butyl and diphenyl amino groups on the flanking phenyl rings. Here, the tolyl substituted derivative was employed to provide optimal solubility properties while still maintaining a convenient NMR spectroscopic handle. Thus, the precursor 2,5-bis-*p*-tolyl-pyrazine (**Tol$_2$Pz**) was synthesized using Suzuki-Miyarua cross-coupling conditions with 2,5-dibromopyrazine and 4-*p*-tolyl-boronic acid[38] (Scheme 1). **Tol$_2$Pz** then underwent an electrophilic borylation with BCl_3 following the synthetic conditions established by the Ingleson group[39] to obtain the dichloroborane **BCl$_2$** in a 51% yield. As previously shown,[22] incorporation of the 2,4,6-fluorinated aryl group on the boron center was key for retaining strong fluorescence so here we again employed this group, along with the fully fluorinated C_6F_5 substituent. Accordingly, arylation of boron with ether-free $ZnAr_2$ (Ar = C_6F_5[40] or 2,4,6-$F_3C_6H_2$[41]) occurs smoothly, yielding the fluoroaryl derivatives **1** and **2**, in 96% and 58%

Scheme 1.

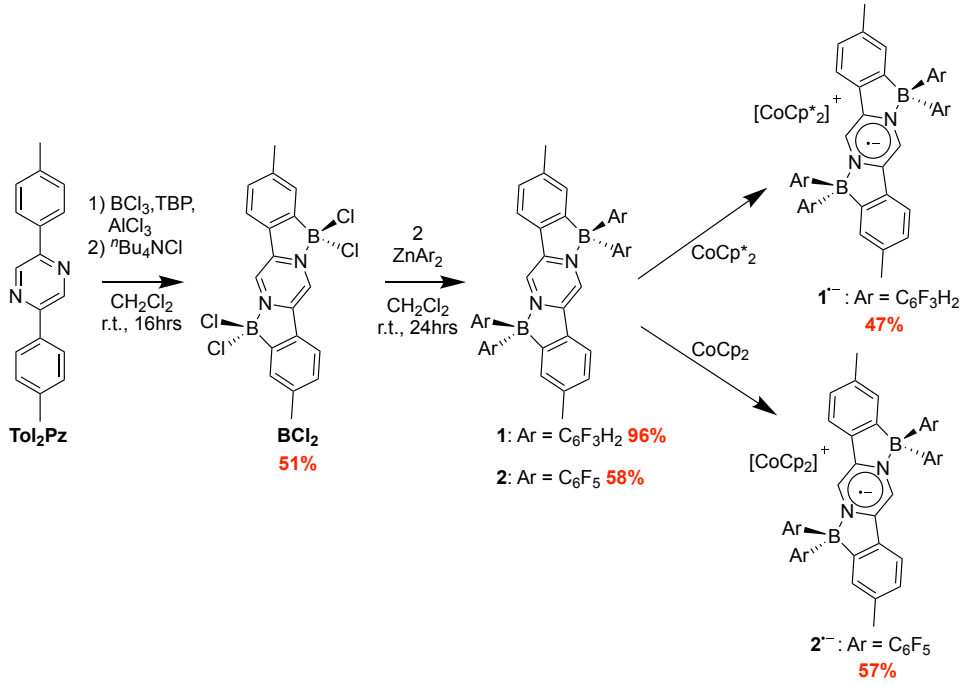

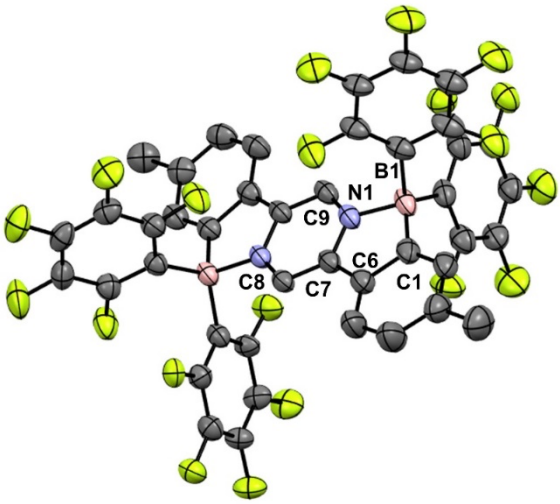

Figure 1. Molecular structure of 2. Hydrogen atoms and solvent have been omitted for clarity. Thermal ellipsoids drawn at 50% probability level. Selected bond lengths (Å) B(1)-N(1) 1.635(3), B(1)-C(1) 1.600(5), C(1)-C(6) 1.407(4), C(6)-C(7) 1.455(4), C(7)-C(8) 1.395(4), N(1)-C(9) 1.321(4), N(1)-C(7) 1.362(4).

yields, respectively. Like previous examples, compounds **1** and **2** are air and moisture stable, bright orange solids that were fully characterized by ^{1}H, ^{19}F, ^{13}C, and ^{11}B NMR spectroscopy (Figure S6-13).[22]

Compound **2** is the first example of a BN dihydroindeno[1,2-b]fluorene incorporating fully fluorinated aryl groups on boron and so was analyzed by X-ray diffraction, with single crystals obtained by a slow evaporation of a concentrated dichloromethane solution. (Figure 1). The solid-state structure was found to incorporate a completely planar pentacyclic core with a B-N bond distance of 1.635(3) Å, closely comparable to the structure of a related derivative previously reported and slightly shorter than the 1.652(1)Å reported for the less conjugated material **IV**[37] (Chart 1). It was observed that the nature of the aryl substituents on boron had a significant effect

on the electronic and photophysical properties of these frameworks.[22] Accordingly, cyclic voltammetry (CV) analysis shows that the less fluorinated compound **1** undergoes a reversible one-electron reduction to the radical anion with a peak potential of -1.03 V (vs $Fc^{0/+}$), with an additional quasi-reversible reduction to the dianion at -2.30 V while the reduction potentials for fully fluorinated **2** are anodically shifted to -0.79 V and -2.10 V, respectively (Figure 2a). At lower scan rates, the second reduction wave becomes less reversible, and in both compounds, there is a small oxidation wave at ca. -0.78 V and -0.63 V for **1** and **2**, respectively. We hypothesize that this oxidation wave arises from an unidentified species resulting from chemical transformation of the dianions formed from two electron reduction. Consistent with this notion is the observation that

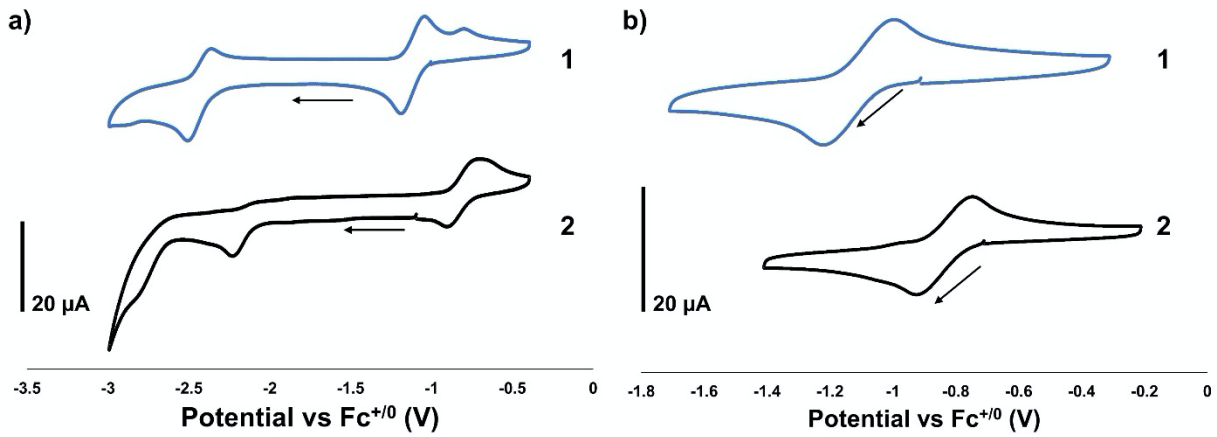

Figure 2. a) Cyclic voltammograms of 1 (top) and 2 (bottom). b) Isolated first reduction wave, demonstrating the absence of the oxidation waves present after second reduction. All CVs were recorded in THF solution with 0.1M *n*Bu_4PF_6 as supporting electrolyte at a scan rate of 500 mV s^{-1}, using a three-electrode setup with glassy carbon, Pt mesh, and Ag/AgCl, working, counter, and reference electrodes, respectively.

the oxidation wave disappears if the scan is halted prior to the second reduction (Figure 2b). From the first reduction potentials, the electrochemical LUMO levels are determined to be -4.31 eV for **1** and -4.07 eV for **2**, relative to the HOMO level of ferrocene (-5.1 eV).[42]

It is clear from the CV experiments that there is a notable change in electron affinity by substituting 2,4,6-$F_3C_6H_2$ aryl groups to C_6F_5 on boron of 0.24 eV. The UV-Vis absorption spectra in dichloromethane demonstrate the same trend with compound **1** and **2** showing their longest wavelength absorption maxima at 476 nm and 497 nm and onset absorptions at 543 nm and 569 nm, respectively (Figure S14). From the onset absorptions, the optical bandgaps are calculated to be 2.28 eV and 2.18 eV for **1** and **2**, respectively. Thus, the stronger electron withdrawing C_6F_5 aryl groups on boron (compound **2**) results in a bathochromic shift in the UV-Vis absorption by 21 nm and a decrease in the optical bandgap of 0.1 eV. It is well reported in the literature that modifying substituents on boron have significant influence on the optoelectronic properties.[22, 37, 43, 44]

To further examine the experimentally determined electronic properties, DFT (PBE0/Def-TZVP) calculated structures and their frontier orbitals are shown in Figure 3. The orbitals are more extensively delocalized across the planar core of the molecules in comparison to those in Pammer's related, but less conjugated materials **IV**. The calculated LUMO energy levels of both **1** and **2** correspond well with LUMO derived from the CV (Table 1) indicating our calculations are in good agreement with experimental results. From **1** to **2**, there is a lowering of the LUMO and HOMO energy levels by 0.43 eV and 0.35 eV, and a decrease in the electronic bandgaps of 1.72 eV and 1.64 eV, respectively.

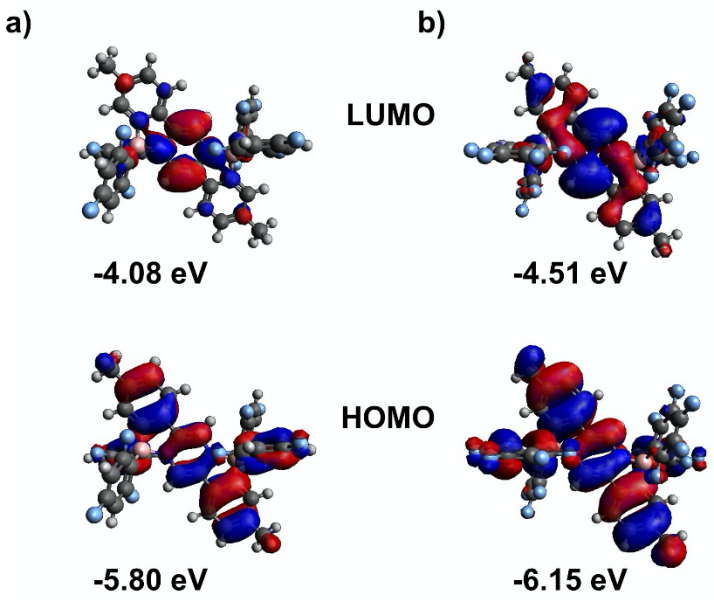

Figure 3. Frontier orbital plots of 1 (a) and 2 (b). Structures were optimized using a PBE0/Def-TZVP level of theory. Orbital plots were generates using Avogadro with an isovalue of 0.01.

Table 1. Electronic properties of compounds 1 and 2.

Compound	$E_{1/2}^{red1}$ (V)	$E_{1/2}^{red2}$ (V)	LUMO[a] (eV)	E_g^{opt}[b] (nm (eV))	LUMO[c] (eV)	HOMO[c] (eV)	E_g[c] (eV)
1	-1.03	-2.30	-4.07	543 (2.28)	-4.08	-5.80	1.72
2	-0.79	-2.10	-4.31	569 (2.18)	-4.51	-6.15	1.64

[a]Relative to the HOMO of ferrocene (-5.1 eV).[42] [b]Based on the absorption onset in dichloromethane solution. [c]DFT calculated frontier orbital energy levels on a PBE0/Def-TZVP level of theory.

Properties of Radical Anion Species. Based on the reversible one-electron reductions of both **1** and **2** as evidenced in the cyclic voltammogram (Figure 1), stable radical anions should be

obtainable via chemical reduction using relatively mild reductants.[45] The reduction of **1** required decamethylcobaltocene ($CoCp^*_2$) while the milder non-methylated cobaltocene ($CoCp_2$) was sufficiently reducing to effect reduction of fully fluorinated compound **2**. With these reductants, the the radical anions $\mathbf{1}^{\bullet-}$ and $\mathbf{2}^{\bullet-}$ were produced in good yields (Scheme 1). Under inert

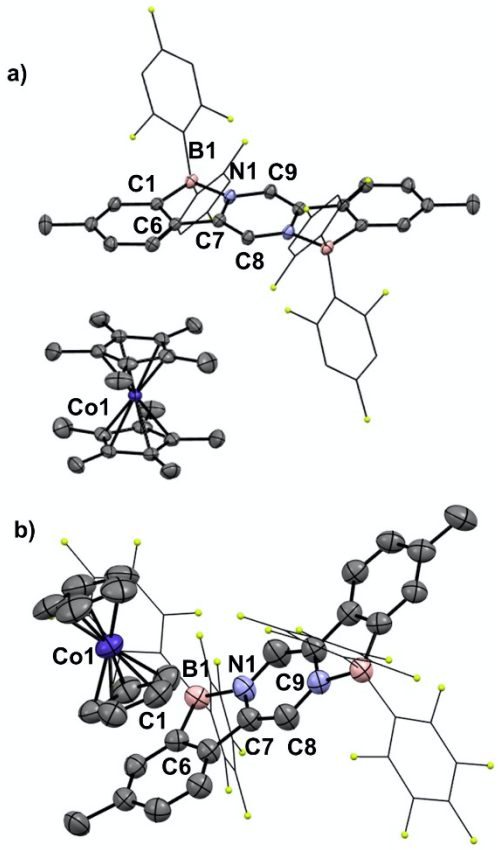

Figure 4. Crystal structures of $1^{\bullet-}$ (a) and $2^{\bullet-}$ (b). Ellipsoids are drawn at the 50% probability level. Hydrogen atoms have been omitted for clarity. Selected metrical data for $1^{\bullet-}$: Bond distances (Å) B(1)-N(1) 1.590(2), B(1)-C(1) 1.618(2), C(1)-C(6) 1.406(2), C(6)-C(7) 1.462(2), C(7)-C(8) 1.364(2), N(1)-C(9) 1.372(2), N(1)-C(7) 1.388(2). Selected metrical data for $2^{\bullet-}$: Bond distances (Å) B(1)-N(1) 1.579(9), B(1)-C(1) 1.629(9), C(1)-C(6) 1.397(8), C(6)-C(7) 1.472(9), C(7)-C(8) 1.370(1), N(1)-C(9) 1.383(9), N(1)-C(7) 1.364(8).

atmosphere, the radical salts were stable over a period of days as solids or as solutions in toluene and dichloromethane. Upon exposure to ambient atmosphere, dark red-purple solutions of the radical anions decolorized to a lighter orange over the course of several minutes. NMR spectroscopic analysis suggest that reoxidation to the neutral compounds **1** and **2** occurred, but that other processes (such as protonation or hydrolysis) were also competitive.

Table 2. Structural data of compounds 1[a], 2, 1$^{\bullet-}$, and 2$^{\bullet-}$, and simulated structures[b].

Compound	Data Type	B(1)-N(1) (Å)	N(1)-C(9) (Å)	N(1)-C(7) (Å)	C(7)-C(8) (Å)
1	X-ray[a]	1.642(6)	1.327(5)	1.348(6)	1.398(6)
2	X-ray	1.635(3)	1.327(4)	1.362(4)	1.389(4)
1$^{\bullet-}$	X-ray	1.590(2)	1.372(2)	1.388(2)	1.364(2)
2$^{\bullet-}$	X-ray	1.579(9)	1.383(9)	1.372(8)	1.370(1)
1	DFT[b]	1.632	1.333	1.371	1.398
2	DFT[b]	1.631	1.333	1.372	1.399
1$^{\bullet-}$	DFT[b]	1.586	1.366	1.394	1.374
2$^{\bullet-}$	DFT[b]	1.582	1.367	1.394	1.374

[a]Crystal data from our previous derivative, with a *tert*-butyl group instead of a methyl group on the phenylpyrazine core. [b]DFT optimized structures calculated on a PBE0/Def-TZVP level of theory.

Both compounds are NMR silent and UV-Vis absorption spectra are shown in Figure S15. The spectra of both radical anions demonstrate a new λ_{max} of 473 nm, demonstrating a hypsochromic shift when compared to the neutral compounds, which is expected due to the single occupancy of the SOMO orbitals. Crystals of both compounds suitable for single crystal X-ray diffraction were grown from dichloromethane/pentane (Figure 4). Since no X-ray diffraction data was collected for **1**, we used data previously reported from our group on the *tert*-butyl substituted derivative on the

phenylpyrazine core[22] for comparison with **1**$^{\bullet-}$. Comparing solid-state structure parameters with those calculated by DFT of the neutral compounds and radical anions there is a clear shortening of the N→B coordination bond and the pyrazine C-C bonds upon reduction, while the pyrazine C-N bonds are elongated (Table 2). Thus, the pyrazine core assumes a quinoidal electron distribution when reduced by one electron,[13, 37] consistent with the character of the LUMO orbitals depicted in Figure 3. Accordingly, the DFT calculated SOMOs of the radical anions are generally similar to the LUMOs of the neutral precursors and reflect the quinoidal character of the pyrazine core (Figure 5).

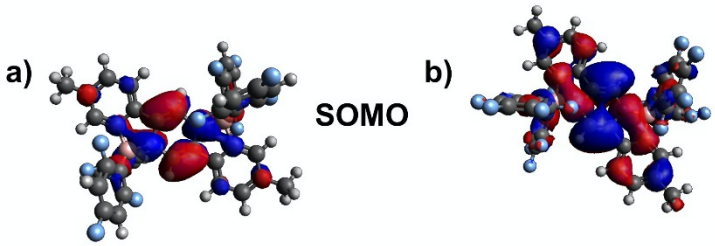

Figure 5. SOMO plots of 1$^{\bullet-}$ (a) and 2$^{\bullet-}$ (b). Structures were optimized using a PBE0/Def-TZVP level of theory. Orbital plots were generates using Avogadro with an isovalue of 0.01.

The radical anions were also characterized by EPR spectroscopy (Figure 6). Both EPR spectra of **1**$^{\bullet-}$ and **2**$^{\bullet-}$ measured in toluene at room temperature displays a complex fine structure (g_{iso} = 2.0041 and 2.0002) that arises from hyperfine coupling with two equivalent boron ($a(^{11}B)$ = 3.20 G and 3.00 G), two nitrogen ($a(^{14}N)$ = 7.39 G and 6.89 G), and two pyrazine hydrogens ($a(^{1}H)$ = 2.92 G and 2.92 G). These ^{14}N and ^{11}B hyperfine couplings are consistent with those found in **IV**[37] and are consistent the SOMOs association with the pyrazine core as indicated by the structural and computational data presented above. The ^{11}B hyperfine coupling constants are also consistent with

other boron heterocyclic radical anions that contain $X_3B{\leftarrow}L$ moieties ($a(^{11}B)$ =2.58 – 3.17 G).[46, 47] When comparing hyperfine coupling data in **1**$^{\bullet-}$ vs **2**$^{\bullet-}$, there is a slight decrease of both the ^{14}N and ^{11}B coupling constants, likely due to the stronger electron-withdrawing effect from C_6F_5 aryl groups that stabilize the charge localization on the pyrazine core.[37]

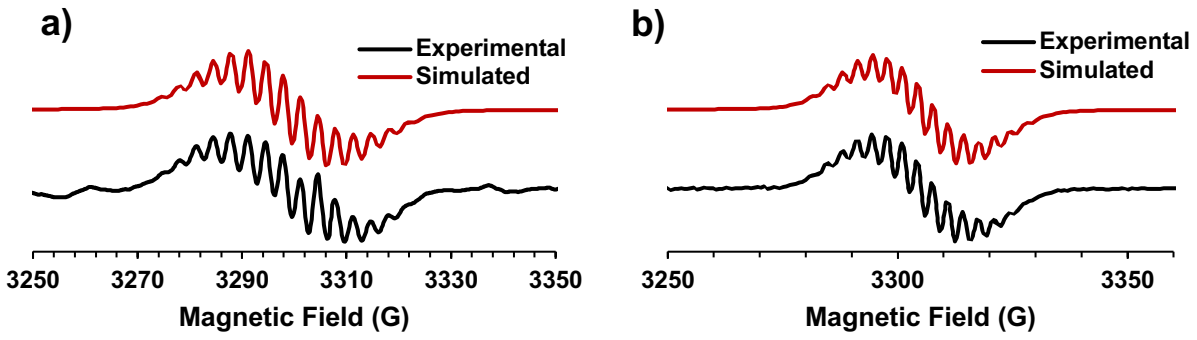

Figure 6. X-band EPR spectra of 1$^{\bullet-}$ (a) and 2$^{\bullet-}$ (b) (~1 mM in toluene at room temperature).

Conclusions

We have previously demonstrated dihydroindeno[1,2-b]fluorene derivatives as acceptors in organic solar cells,[22] but with relatively low efficiencies. The incorporation of electron withdrawing capping groups[48-50] at the position of substitution on the flanking phenyl groups are a potential means of improving the performance of these materials but prior to embarking on such efforts, the stability of the reduced compounds was undertaken. Here we have demonstrated that the radical anions formed are stable towards dimerization (intrinsic degradation) but likely need to be protected from extrinsic degradation processes. The stability of the radical anions towards dimerization is related to the substantial localization of charge in the pyrazine core (as demonstrated by structural, spectroscopic and computational studies) and the steric protection

afforded by the aryl groups on boron. We also show that the reduction potential can be lowered to a minimum by tuning the electron accepting ability with the incorporation more electron-withdrawing C_6F_5 aryl groups on boron. This results in an anodic shift in the electron reductions by ca. 0.2 V, a bathochromic shift in the absorption by 26 nm, and a decrease in the calculated electronic bandgap by 12 eV (Table 1). We are currently working on elaborating these cores to develop higher performing acceptors for organic solar cells.

Experimental Section

See the supporting information for a full description of experimental procedures and compound characterization data.

Acknowledgements

Funding for this work was provided by NSERC of Canada in the form of a Discovery Grant to W.E.P. W.E.P. also thanks the Canada Research Chair secretariat for a Tier I CRC (2020−2027). T. N. acknowledges the Province of Alberta for an Alberta Graduate Excellence Scholarship (AGES).

Supporting Information Available: Details on general methods, syntheses and characterization of ligands and catalyst precursors and the procedures employed for the metathesis reactions. CCDC 2127347-2127349 contain the supplementary crystallographic data for the structures of **2**, $\mathbf{2}^{\bullet-}$ and $\mathbf{1}^{\bullet-}$, respectively. These data can be obtained, free of charge, via www.ccdc.cam.ac.uk/conts/retrieving.html (or from the Cambridge Crystallographic Data Centre, 12 Union Road, Cambridge CB2 1EZ, UK (Fax: 44-1223-336033 or e-mail: deposit@ccdc.cam.ac.uk)).

References

1. Bosdet, M. J. D.; Piers, W. E. B-N as a C-C substitute in aromatic systems. *Can. J. Chem.* **2009,** *87*, 8-29.
2. Liu, Z.; Marder, T. B. B□N versus C□C: How Similar Are They? *Angew. Chem. Int. Ed.* **2008,** *47*, 242-244.
3. Campbell, P. G.; Marwitz, A. J. V.; Liu, S.-Y. Recent Advances in Azaborine Chemistry. *Angew. Chem. Int. Ed.* **2012,** *51*, 6074-6092.
4. Wang, X.-Y.; Wang, J.-Y.; Pei, J. BN Heterosuperbenzenes: Synthesis and Properties. *Chem. Eur. J.* **2015,** *21*, 3528-3539.
5. Helten, H. B=N Units as Part of Extended pi-Conjugated Oligomers and Polymers. *Chem.-Eur. J.* **2016,** *22*, 12972-12982.
6. Hou, Q.; Liu, L.; Mellerup, S. K.; Wang, N.; Peng, T.; Chen, P.; Wang, S. Stimuli-Responsive B/N Lewis Pairs Based on the Modulation of B-N Bond Strength. *Org. Lett.* **2018,** *20*, 6467-6470.
7. Yang, D. T.; Mellerup, S. K.; Peng, J. B.; Wang, X.; Li, Q. S.; Wang, S. Substituent Directed Phototransformations of BN-Heterocycles: Elimination vs Isomerization via Selective B-C Bond Cleavage. *J. Am. Chem. Soc.* **2016,** *138*, 11513-11516.
8. Giustra, Z. X.; Liu, S.-Y. The State of the Art in Azaborine Chemistry: New Synthetic Methods and Applications. *J. Am. Chem. Soc.* **2018,** *140*, 1184-1194.
9. Mellerup, S. K.; Wang, S. Boron-Doped Molecules for Optoelectronics. *Trends in Chemistry* **2019,** *1*, 77-89.
10. Kondo, Y.; Yoshiura, K.; Kitera, S.; Nishi, H.; Oda, S.; Gotoh, H.; Sasada, Y.; Yanai, M.; Hatakeyama, T. Narrowband deep-blue organic light-emitting diode featuring an organoboron-based emitter. *Nature Photonics* **2019,** *13*, 678-682.
11. Emslie, D. J. H.; Piers, W. E.; Parvez, M. 2,2 '-diborabiphenyl: A Lewis acid analogue of 2,2 '-bipyridine. *Angew. Chem. Int. Ed.* **2003,** *42*, 1252-1255.
12. Jaska, C. A.; Emslie, D. J. H.; Bosdet, M. J. D.; Piers, W. E.; Sorensen, T. S.; Parvez, M. Triphenylene analogues with B2N2C2 cores: Synthesis, structure, redox behavior, and photophysical properties. *J. Am. Chem. Soc.* **2006,** *128*, 10885-10896.
13. Zhu, C.; Ji, X.; You, D.; Chen, T. L.; Mu, A. U.; Barker, K. P.; Klivansky, L. M.; Liu, Y.; Fang, L. Extraordinary Redox Activities in Ladder-Type Conjugated Molecules Enabled by B ← N Coordination-Promoted Delocalization and Hyperconjugation. *J. Am. Chem. Soc.* **2018,** *140*, 18173-18182.
14. Bosdet, M. J. D.; Piers, W. E.; Sorensen, T. S.; Parvez, M. 10a-Aza-10b-borapyrenes: Heterocyclic analogues of pyrene with internalized BN moieties. *Angew. Chem. Int. Ed.* **2007,** *46*, 4940-4943.
15. Zhang, P.-F.; Zeng, J.-C.; Zhuang, F.-D.; Zhao, K.-X.; Sun, Z.-H.; Yao, Z.-F.; Lu, Y.; Wang, X.-Y.; Wang, J.-Y.; Pei, J. Parent B2N2-Perylenes with Different BN Orientations. *Angew. Chem. Int. Ed.* **2021,** *60*, 23313-23319.
16. Oda, S.; Hatakeyama, T. Development of One-Shot/One-Pot Borylation Reactions toward Organoboron-Based Materials. *Bulletin of the Chemical Society of Japan* **2021,** *94*, 950-960.
17. Escande, A.; Ingleson, M. J. Fused polycyclic aromatics incorporating boron in the core: fundamentals and applications. *Chem. Commun.* **2015,** *51*, 6257-6274.
18. Neue, B.; Araneda, J. F.; Piers, W. E.; Parvez, M. BN-Dibenzo[a,o]picenes: Analogues of an Unknown Polycyclic Aromatic Hydrocarbon. *Angew. Chem. Int. Ed.* **2013,** *52*, 9966-9969.

19. Dewar, M. J. S.; Kubba, V. P.; Pettit, R. 624. New heteroaromatic compounds. Part I. 9-Aza-10-boraphenanthrene. *J. Chem. Soc.* **1958**, 3073-3076.
20. Morgan, M. M.; Piers, W. E. Efficient synthetic methods for the installation of boron-nitrogen bonds in conjugated organic molecules. *Dalton Trans.* **2016,** *45*, 5920-5924.
21. Wang, Y.; Wang, N.; Yang, Q.; Zhang, J.; Liu, J.; Wang, L. A polymer acceptor containing the B←N unitfor all-polymer solar cells with 14% efficiency. *Journal of Materials Chemistry A* **2021,** *9*, 21071-21077.
22. Morgan, M. M.; Nazari, M.; Pickl, T.; Rautiainen, J. M.; Tuononen, H. M.; Piers, W. E.; Welch, G. C.; Gelfand, B. S. Boron–nitrogen substituted dihydroindeno[1,2- b]fluorene derivatives as acceptors in organic solar cells. *Chem. Commun.* **2019,** *55*, 11095-11098.
23. Mateker, W. R.; McGehee, M. D. Progress in Understanding Degradation Mechanisms and Improving Stability in Organic Photovoltaics. *Advanced Materials* **2017,** *29*, 1603940-1603940.
24. Inasaridze, L. N.; Shames, A. I.; Martynov, I. V.; Li, B.; Mumyatov, A. V.; Susarova, D. K.; Katz, E. A.; Troshin, P. A. Light-induced generation of free radicals by fullerene derivatives: an important degradation pathway in organic photovoltaics? *Journal of Materials Chemistry A* **2017,** *5*, 8044-8050.
25. Yamilova, O. R.; Martynov, I. V.; Brandvold, A. S.; Klimovich, I. V.; Balzer, A. H.; Akkuratov, A. V.; Kusnetsov, I. E.; Stingelin, N.; Troshin, P. A. What is Killing Organic Photovoltaics: Light-Induced Crosslinking as a General Degradation Pathway of Organic Conjugated Molecules. *Advanced Energy Materials* **2020,** *10*, 1903163-1903163.
26. Hoefelmeyer, J. D.; Gabbaï, F. P. An Intramolecular Boron−Boron One-Electron σ-Bond. *J. Am. Chem. Soc.* **2000,** *122*, 9054-9055.
27. Kwaan, R. J.; Harlan, C. J.; Norton, J. R. Generation and characterization of the tris(pentafluorophenyl)borane radical anion. *Organometallics* **2001,** *20*, 3818-3820.
28. Araneda, J. F.; Piers, W. E.; Sgro, M. J.; Parvez, M. Ring Expansion Reactions of Electron-Rich Boron-Containing Heterocycles. *Organometallics* **2015,** *34*, 3408-3413.
29. von Grotthuss, E.; Prey, S. E.; Bolte, M.; Lerner, H. W.; Wagner, M. Selective CO2 Splitting by Doubly Reduced Aryl Boranes to Give CO and [CO3]2−. *Angewandte Chemie - International Edition* **2018,** *57*, 16491-16495.
30. Budy, H.; Gilmer, J.; Trageser, T.; Wagner, M. Anionic Organoboranes: Delicate Flowers Worth Caring for. *Eur. J. Inorg. Chem.* **2020,** *2020*, 4148-4162.
31. Taniguchi, T. Advances in chemistry of N-heterocyclic carbene boryl radicals. *Chemical Society Reviews* **2021,** *50*, 8995-9021.
32. Ashley, A. E.; Herrington, T. J.; Wildgoose, G. G.; Zaher, H.; Thompson, A. L.; Rees, N. H.; Krämer, T.; O'Hare, D. Separating Electrophilicity and Lewis Acidity: The Synthesis, Characterization, and Electrochemistry of the Electron Deficient Tris(aryl)boranes B(C6F5)3–n(C6Cl5)n (n = 1–3). *J. Am. Chem. Soc.* **2011,** *133*, 14727-14740.
33. Wood, T. K.; Piers, W. E.; Keay, B. A.; Parvez, M. Spirocyclic boronium ions: precursors to persistent neutral radicals. *Chem. Commun.* **2009**, 5147-5149.
34. Scholz, A. S.; Massoth, J. G.; Bursch, M.; Mewes, J.-M.; Hetzke, T.; Wolf, B.; Bolte, M.; Lerner, H.-W.; Grimme, S.; Wagner, M. BNB-Doped Phenalenyls: Modular Synthesis, Optoelectronic Properties, and One-Electron Reduction. *J. Am. Chem. Soc.* **2020,** *142*, 11072-11083.
35. Mondol, R.; Snoeken, D. A.; Chang, M. C.; Otten, E. Stable, crystalline boron complexes with mono-, di- and trianionic formazanate ligands. *Chem. Commun.* **2017,** *53*, 513-516.

36. Van Belois, A.; Maar, R. R.; Workentin, M. S.; Gilroy, J. B. Dialkynylborane Complexes of Formazanate Ligands: Synthesis, Electronic Properties, and Reactivity. *Inorganic Chemistry* **2019,** *58*, 834-843.
37. Grandl, M.; Rudolf, B.; Sun, Y.; Bechtel, D. F.; Pierik, A. J.; Pammer, F. Intramolecular N→B Coordination as a Stabilizing Scaffold for π-Conjugated Radical Anions with Tunable Redox Potentials. *Organometallics* **2017,** *36*, 2527-2535.
38. Culham, S.; Lanoë, P.-H.; Whittle, V. L.; Durrant, M. C.; Williams, J. A. G.; Kozhevnikov, V. N. Highly Luminescent Dinuclear Platinum(II) Complexes Incorporating Bis-Cyclometallating Pyrazine-Based Ligands: A Versatile Approach to Efficient Red Phosphors. *Inorganic Chemistry* **2013,** *52*, 10992-11003.
39. Crossley, D. L.; Cid, J.; Curless, L. D.; Turner, M. L.; Ingleson, M. J. Facile Arylation of Four-Coordinate Boron Halides by Borenium Cation Mediated Boro-desilylation and -destannylation. *Organometallics* **2015,** *34*, 5767-5774.
40. Sun, Y. M.; Piers, W. E.; Parvez, M. The solid-state structure of bis(pentafluorophenyl)zinc. *Can. J. Chem.* **1998,** *76*, 513-517.
41. Al-Khafaji, Y. F.; Elsegood, M. R. J.; Frese, J. W. A.; Redshaw, C. Ring opening polymerization of lactides and lactones by multimetallic alkyl zinc complexes derived from the acids Ph2C(X)CO2H (X = OH, NH2). *RSC Advances* **2017,** *7*, 4510-4517.
42. Cardona, C. M.; Li, W.; Kaifer, A. E.; Stockdale, D.; Bazan, G. C. Electrochemical considerations for determining absolute frontier orbital energy levels of conjugated polymers for solar cell applications. *Advanced Materials* **2011,** *23*, 2367-2371.
43. Yusuf, M.; Liu, K.; Guo, F.; Lalancette, R. A.; Jäkle, F. Luminescent organoboron ladder compounds via directed electrophilic aromatic C-H borylation. *Dalton Trans.* **2016,** *45*, 4580-4587.
44. Shao, X.; Dou, C.; Liu, J.; Wang, L. A new building block with intramolecular D-A character for conjugated polymers: ladder structure based on B←N unit. *Science China Chemistry* **2019,** *62*, 1387-1392.
45. Connelly, N. G.; Geiger, W. E. Chemical redox agents for organometallic chemistry. *Chemical Reviews* **1996,** *96*, 877-910.
46. Longobardi, L. E.; Liu, L.; Grimme, S.; Stephan, D. W. Stable Borocyclic Radicals via Frustrated Lewis Pair Hydrogenations. *J. Am. Chem. Soc.* **2016,** *138*, 2500-2503.
47. Feng, Z.; Chong, Y.; Tang, S.; Ruan, H.; Fang, Y.; Zhao, Y.; Jiang, J.; Wang, X. Stable Boron-Containing Blue-Photoluminescent Radicals. *Chinese Journal of Chemistry* **2021,** *39*, 1297-1302.
48. Yuan, J.; Zhang, Y.; Zhou, L.; Zhang, G.; Yip, H.-L.; Lau, T.-K.; Lu, X.; Zhu, C.; Peng, H.; Johnson, P. A.; Leclerc, M.; Cao, Y.; Ulanski, J.; Li, Y.; Zou, Y. Single-Junction Organic Solar Cell with over 15% Efficiency Using Fused-Ring Acceptor with Electron-Deficient Core. *Joule* **2019,** *3*, 1140-1151.
49. Lin, Y.; Wang, J.; Zhang, Z.-G.; Bai, H.; Li, Y.; Zhu, D.; Zhan, X. An Electron Acceptor Challenging Fullerenes for Efficient Polymer Solar Cells. *Advanced Materials* **2015,** *27*, 1170-1174.
50. Liu, W.; Xu, X.; Yuan, J.; Leclerc, M.; Zou, Y.; Li, Y. Low-Bandgap Non-fullerene Acceptors Enabling High-Performance Organic Solar Cells. *ACS Energy Letters* **2021,** *6*, 598-608.

Supporting Information

Stable, π-conjugated radical anions of boron-nitrogen dihydroindeno[1,2-b]fluorenes

Tony Nguyen, Tyler J. Hannah, Warren E. Piers* and Benjamin S. Gelfand

University of Calgary, Department of Chemistry, 2500 University Drive N.W., Calgary, Alberta, Canada, T2N 1N4

Contents

Experimental Details

General Considerations.

All experiments were performed under a purified argon atmosphere either using a MBraun Unilab glove box or a double manifold high vacuum line following standard techniques, unless otherwise specified. Reactions were performed on a double manifold high vacuum line fitted with an OxisorBW scrubber (Matheson Gas products) argon purification cartridge, using standard techniques.

Hexanes, pentane, tetrahydrofuran, diethyl ether, and toluene were dried and purified using a Grubbs/Dow solvent purification system and stored in 500ml thick-walled Kontes flasks over sodium/benzophenone ketal. CH_2Cl_2 was stored in the same manner except dried over calcium dihydride instead of sodium/benzophenone ketal. All dried solvents were degassed, and vacuum distilled prior to use. All other commercially available starting materials were used without further purification. $Zn(C_6F_3H_2)_2$ and $Zn(C_6F_5)_2$ was prepared as previously reported.[1]

NMR were obtained using a Bruker Ascend-500 NMR spectrometer. ^1H and ^{13}C NMR chemical shifts were referenced to residual solvent protons and naturally abundant ^{13}C resonances for all deuterated solvents. Absorption spectra were measured using a Varian Cary-50 single beam spectrophotometer. X-ray crystallographic analyses were performed by Dr. Benjamin Gelfand on a Nonius system equipped with a Bruker Apex-II CCD detector using samples coated in Fomblin Y HVAC 140/13 oil and mounted on a glass fibre. Full crystallography details can be found in independently uploaded .cif files CCDC 2127347-2127349. Cyclic voltammetry was collected with a CHI660D potentiostat using a three-electrode setup using a CHI660D potentiostat. Glassy carbon, platinum wire, and silver wire were used as the working, counter, and reference electrodes, respectively. Ionic strength of the solution was maintained by using a 0.1M solution of

$[nBu_4N][PF_6]$ in THF solvent. All cyclic voltammograms were referenced to the Fc/Fc^+. Elemental and mass spectrometric analyses were performed by staff at the Instrumentation Facility in the Department of Chemistry, University of Calgary.

X-band EPR spectra (9.34 GHz) were recorded on a Bruker EMX 10/12 spectrometer equipped with VT capabilities with a 10-inch magnet and a 12 kV power supply. Spectra were recorded in toluene with the following parameters: 0.6325 mW power, 20 dB attenuation, 0.5 G modulation amplitude, 100 kHz modulation frequency, 30 s sweep time, 200 G sweep width, 5.12 s time constant, 30 ms conversion time, 9.272×10^{-9} conversion factor, 74 dB gain over 32 scans. Spectra were simulated with EasySpin.[2]

Geometries of minimum structures and transition states were optimized with Gaussian 09 program package[C1] using PBE0 hybrid density functional[C2] and Ahlrichs' small triple-ζ valence quality def-TZVP basis sets.[C3] Nature of the stationary points was ascertained by frequency calculations and none of the optimized structures showed negative eigenfrequencies.

C1 M. J. Frisch, G. W. Trucks, H. B. Schlegel, G. E. Scuseria, M. A. Robb, J. R. Cheeseman, G. Scalmani, V. Barone, B. Mennucci, G. A. Petersson, H. Nakatsuji, M. Caricato, X. Li, H. P. Hratchian, A. F. Izmaylov, J. Bloino, G. Zheng, J. L. Sonnenberg, M. Hada, M. Ehara, K. Toyota, R. Fukuda, J. Hasegawa, M. Ishida, T. Nakajima, Y. Honda, O. Kitao, H. Nakai, T. Vreven, J. A. Montgomery Jr., J. E. Peralta, F. Ogliaro, M. Bearpark, J. J. Heyd, E. Brothers, K. N. Kudin, V. N. Staroverov, R. Kobayashi, J. Normand, K. Raghavachari, A. Rendell, J. C. Burant, S. S. Iyengar, J. Tomasi, M. Cossi, N. Rega, M. J. Millam, M. Klene, J. E. Knox, J. B. Cross, V. Bakken, C. Adamo, J. Jaramillo, R. Gomperts, R. E. Stratmann, O. Yazyev, A. J. Austin, R. Cammi, C. Pomelli, J. W. Ochterski, R. L. Martin, K. Morokuma, V. G. Zakrzewski, G. A. Voth, P. Salvador, J. J. Dannenberg, S. Dapprich, A. D. Daniels, Ö.; Farkas, J. B. Foresman, J. V. Ortiz, J. Cioslowski and D. J. Fox, GAUSSIAN 09 (Revision D.01), Gaussian, Inc., Wallingford CT, 2013.

C2 (a) J. P. Perdew, K. Burke and M. Ernzerhof, Phys. Rev. Lett., 1996, 77, 3865–3868; Erratum, Phys. Rev. Lett., 1997, 78, 1396; (b) J. P. Perdew, M. Ernzerhof and K. Burke, J. Chem. Phys., 1996, 105, 9982–9985; (c) C. Adamo and V. Barone, J. Chem. Phys., 1999, 110, 6158–6170.

C3 A. Schaefer, C. Huber and R. Ahlrichs, J. Chem. Phys., 1994, 100, 5829−5836

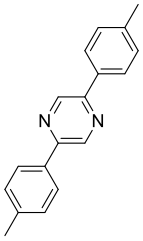

Synthesis of 2,5-di-*p*-tolylpyrazine (Tol2Pz): Synthesis was adapted using previously reported procedures.[3] 4-methylphenyl boronic acid (3.01 g, 19.5 mmol) and 2,5-dibromopyrazine (1.78 g, 7.5 mmol) were dissolved in 1,4-dioxane (60 mL). This solution was then degassed with argon for 10 minutes. To this was added $Pd(PPh_3)_4$ (0.52 g, 0.5 mmol) and a solution of potassium carbonate (6.2 g, 45.0 mmol) in water (20 mL). This solution was further degassed for 10 minutes. This was then refluxed under an atmosphere of argon for 16 hours. The solution was then cooled to room temperature and the resulting yellow solid was collected by filtration, washing with water (50 mL) and hexanes (50 mL). The solid was recrystallized in hot ethanol, giving a white solid in 89 % yield (1.65 g, 6.7 mmol).

^{1}H NMR (500 MHz $CDCl_3$) δ 9.03 (s, 2H), 7.96 (d, J = 8.3 Hz, 4H), 7.33 (d, J = 8 Hz, 4H), 2.44 (s, 6H).

^{13}C {^{1}H} NMR (126 MHz, $CDCl_3$) δ 150.51, 141.08, 139.99, 133.71, 129.93, 126.73, 21.52.

ESI: m/z $[M+H]^+$ calcd for $C_{18}H_{17}N_2$, 261.13862; found 261.13976.

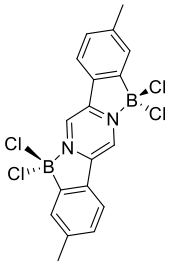

Synthesis of BCl_2: Synthesis was adapted using previously reported procedures.[4] 2,5-bis(p-tolyl)pyrazine (**Tol2Pz**) (600 mg, 2.43 mmol) and 2,6-di-tertbutylpyridine (928 mg, 4.85 mmol) were dissolved in dry CH_2Cl_2 (50 mL) under an atmosphere of argon. A solution of BCl_3 in CH_2Cl_2 (1 M, 6.1 mmol) was added dropwise resulting in a color change to bright red. $AlCl_3$ (1.29 g, 9.70 mmol) was then added resulting in another color change to dark purple. This mixture was stirred under argon for 16 hours.

Tetrabutylammonium chloride (1.35 g, 4.85 mmol) was added to this, and it was stirred for an additional hour. Solvent was then removed under vacuum and the resulting purple solid was washed with water (150 mL), hexanes (150 mL), and DCM (20 mL). The purple solid was collected in 51 % yield (522 mg, 1.24 mmol).

^{1}H NMR (500 MHz, Acetone-d_6) δ 9.93 (s, 2H), 8.44 (d, J = 8.0 Hz, 2H), 7.57 (d, J = 1.6 Hz, 2H), 7.42 (d, J = 8.0 Hz, 2H), 2.50 (s, 6H).

^{11}B NMR (161 MHz, Acetone-d_6) δ 8.23.

^{13}C {^{1}H} NMR (126 MHz, Acetone-d_6) δ 150.52, 144.46, 136.18, 129.97, 129.71, 129.06, 123.41, 20.60. (Signal for carbon attached to boron on phenylpyrazine core not observed).

EI: m/z [M^+] calcd for $C_{18}H_{14}B_2N_2Cl_4$, 422.0068; found 422.0045.

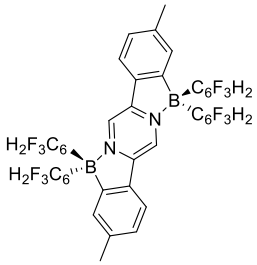

Synthesis of 1: Synthesis was adapted using previously reported procedures.[5] A round-bottom flask was loaded with **BCl_2** (100 mg, 0.24 mmol) and ether-free $Zn(C_6F_3H_2)_2$ (167 mg, 0.51 mmol) were both added to a round-bottom flask, and CH_2Cl_2 was distilled into the reaction vessel. The mixture was stirred for 2 hours resulting in a fluorescent yellow solution. The solution was passed through a silica plug and dried under high vacuum yielding a bright orange solid in 96% yield (190 mg, 0.24 mmol).

^{1}H NMR (500 MHz, $CDCl_3$) δ 9.20 (s, 2H), 7.73 (d, J = 8.0 Hz, 2H), 7.58 (s, 1H), 7.21 (d, J = 7.9 Hz, 2H), 6.52 (t, J = 8.5 Hz, 8H), 2.42 (s, 6H).

^{19}F NMR (471 MHz, $CDCl_3$) δ -98.65 (d, J = 7.6 Hz), -112.40.

^{13}C {^{1}H} NMR (126 MHz, $CDCl_3$) δ 165.59 (dt, $^{1}J_{CF}$ = 243 Hz, $^{3}J_{CF}$ = 16 Hz), 162.34 (dt, $^{1}J_{CF}$ = 247.6, 17 Hz), 160.31, 151.38, 144.09, 135.94, 131.66, 129.40, 128.62, 121.85, 115.31, 100.24 (dd, J = 33.9, 24.0 Hz), 22.46.

^{11}B NMR (161 MHz, $CDCl_3$) δ 0.13.

MALDI: m/z $[M]^+$ calcd for $C_{42}H_{22}B_2F_{12}N_2$, 804.1772; found 804.1763.

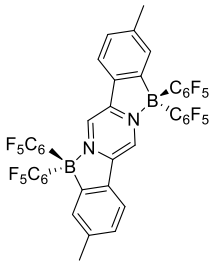

Synthesis of 2: A round-bottom flask was loaded with **BCl_2** (100mg, 0.24 mmol) and ether-free $Zn(C_6F_5)_2$ (237 mg, 0.59 mmol) were both added to a round-bottom flask, and CH_2Cl_2 was distilled into the reaction vessel. The mixture was stirred for 24 hours resulting in a fluorescent orange solution. The solution was passed through a silica plug and dried under high vacuum yielding a bright orange solid. X-ray suitable crystals were obtained by a slow evaporation of a saturated dichloromethane solution at room temperature to yield bright orange plates (130 mg, 0.14 mmol, 58% yield).

^{1}H NMR (500 MHz, CD_2Cl_2) δ 9.19 (s, 2H), 7.84 (d, J = 8.1 Hz, 2H), 7.57 (s, 1H), 7.30 (d, J = 7.2 Hz), 2.42 (s, 6H).

^{19}F NMR (471 MHz, CD_2Cl_2) δ -132.40 (d, J = 16.8 Hz, 2F), -157.63 (t, J = 20.5 Hz, 1F), -163.82 (m, 1F).

^{13}C {^{1}H} NMR (126 MHz, $CDCl_3$) δ 151.89, 147.96 (d, $^{1}J_{CF}$ = 240 Hz), 145.59, 140.53 (d, $^{1}J_{CF}$ = 258 Hz), 137.66 (d, $^{1}J_{CF}$ = 258 Hz), 136.15, 131.75, 129.63, 129.07, 122.52, 115.33, 22.53. (Signal for carbon attached to boron on phenylpyrazine core not observed).

^{11}B NMR (161 MHz $CDCl_3$) δ 0.46.

ESI: m/z $[M^{\bullet}]^-$ calcd for $C_{42}H_{14}B_2F_{20}N_2$, 948.10292; found 948.10687.

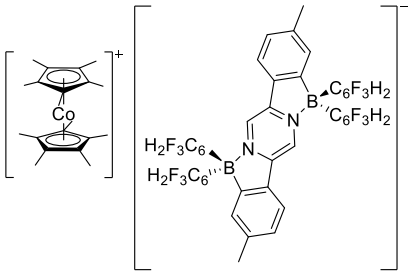

Synthesis of 1•−: Compound **1** (5.1 mg, 0.006 mmol) was dissolved in 2 mL of CH_2Cl_2 and $CoCp_2$ (4.1 mg, 0.012 mmol) was added to the solution and stirred for 2 hours. Solvent was removed under high vacuum, resulting in an oily residue, which was washed with pentane to remove any residual CH_2Cl_2. The residue was extracted with toluene and filtered, solvent was removed under high vacuum, resulting in a dark purple solid. The solution was filtered, and recrystallized from a dichloromethane/pentane solvent mixture, resulting in dark purple crystals with a yield of 47% (3.2 mg, 0.003 mmol).

Elemental analysis: Calcd C 65.59; H 4.62; N 2.47. Found C 65.92; H 4.30; N 2.40.

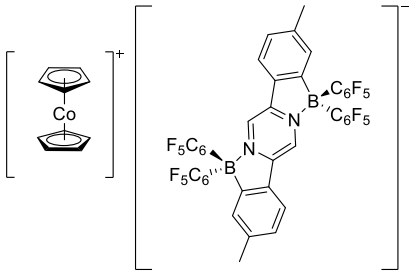

Synthesis of 2•−: Compound **2** (10 mg, 0.01 mmol) was dissolved in 2 mL of CH_2Cl_2 and $CoCp_2$ (4 mg, 0.02 mmol) was added to the mixture and stirred for 2 hours, resulting in a dark orange solution. Solvent was removed under high vacuum, resulting in an oily residue, which was washed with pentane to remove any residual CH_2Cl_2. The residue was extracted with toluene and filtered, toluene was removed under high vacuum, resulting in a dark purple-brown solid. X-ray suitable crystals were obtained by slow diffusion of pentane into dichloromethane solution, resulting in dark purple needles with a yield of 57% (6.8 mg, 0.006 mmol).

Elemental analysis: Calcd C 54.92; H 2.13; N 2.46. Found C 54.91; H 2.45; N 2.48.

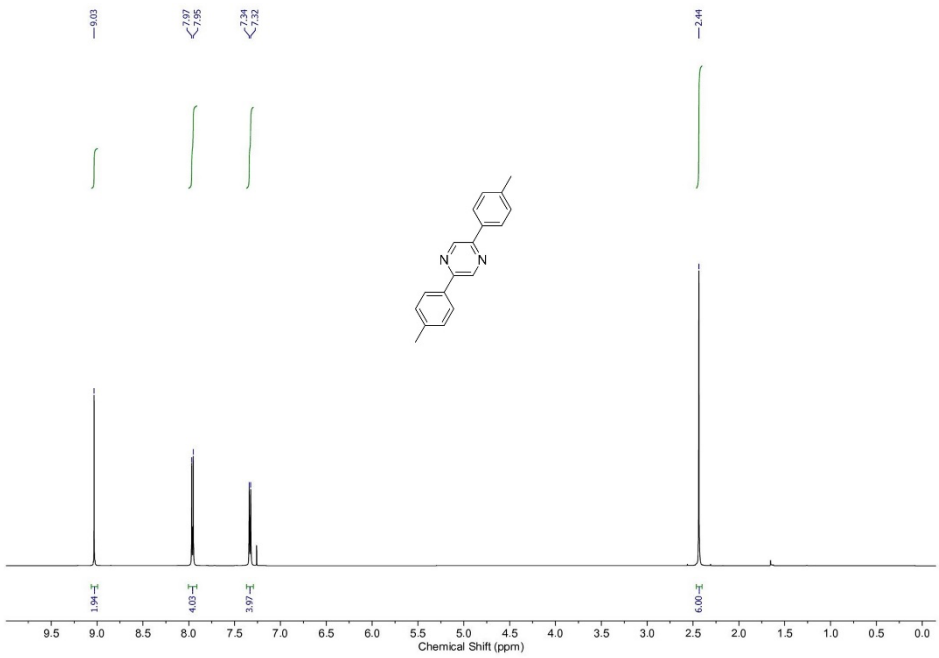

Figure S1. ^{1}H NMR of **Tol2Pz** in $CDCl_3$

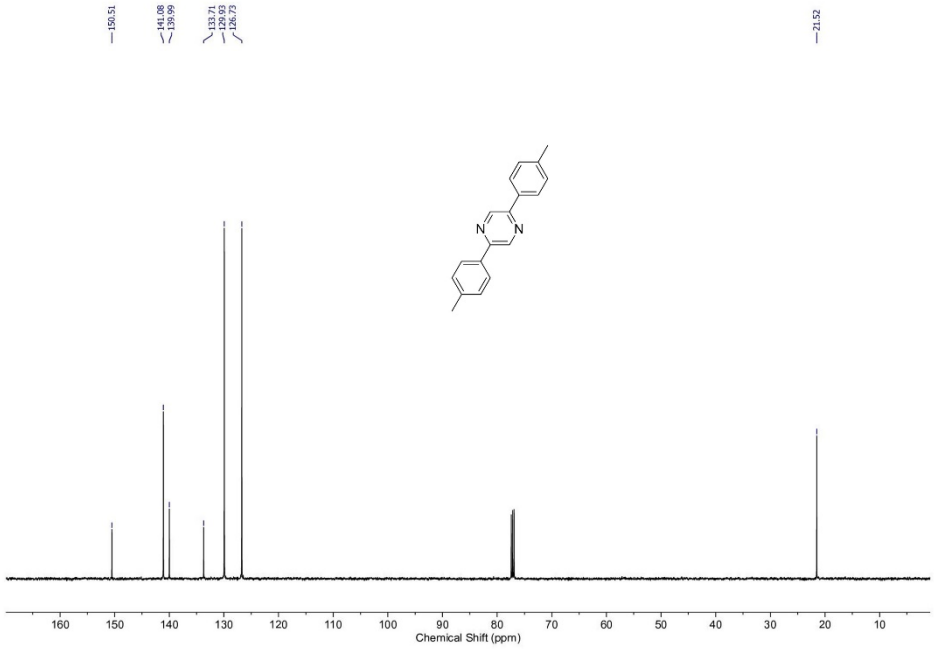

Figure S2. ^{13}C {^{1}H} NMR of **Tol2Pz** in $CDCl_3$

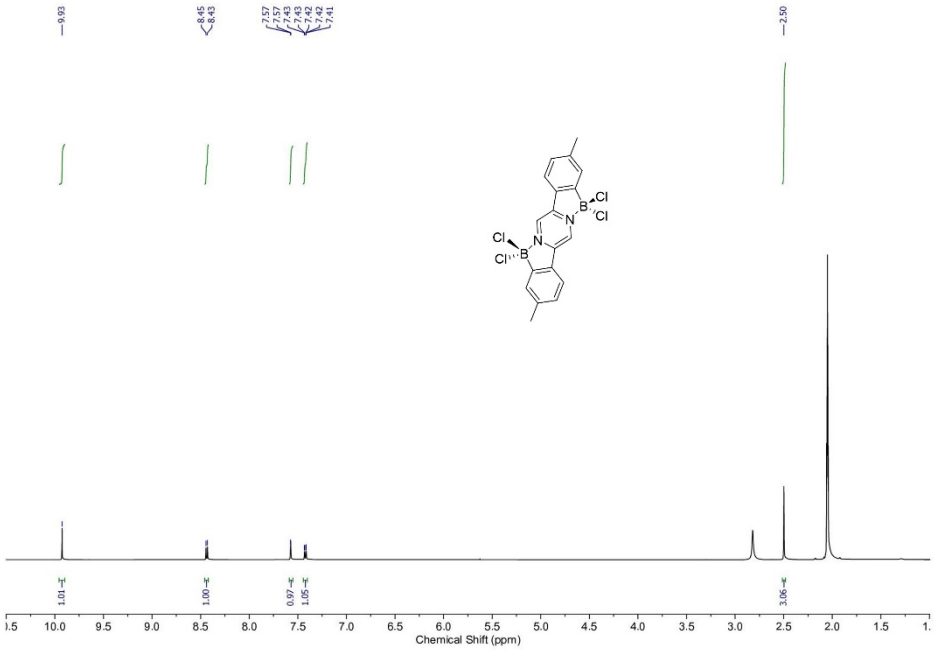

Figure S3. ^{1}H NMR of **BCl$_2$** in Acetone-d$_6$

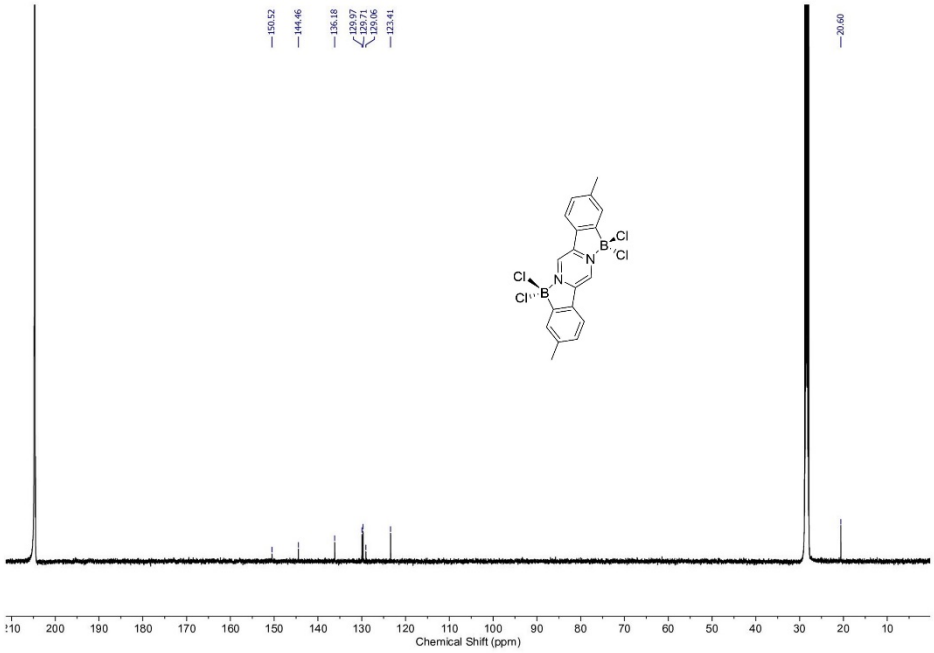

Figure S4. ^{13}C {^{1}H} NMR of **BCl$_2$** in Acetone-d$_6$

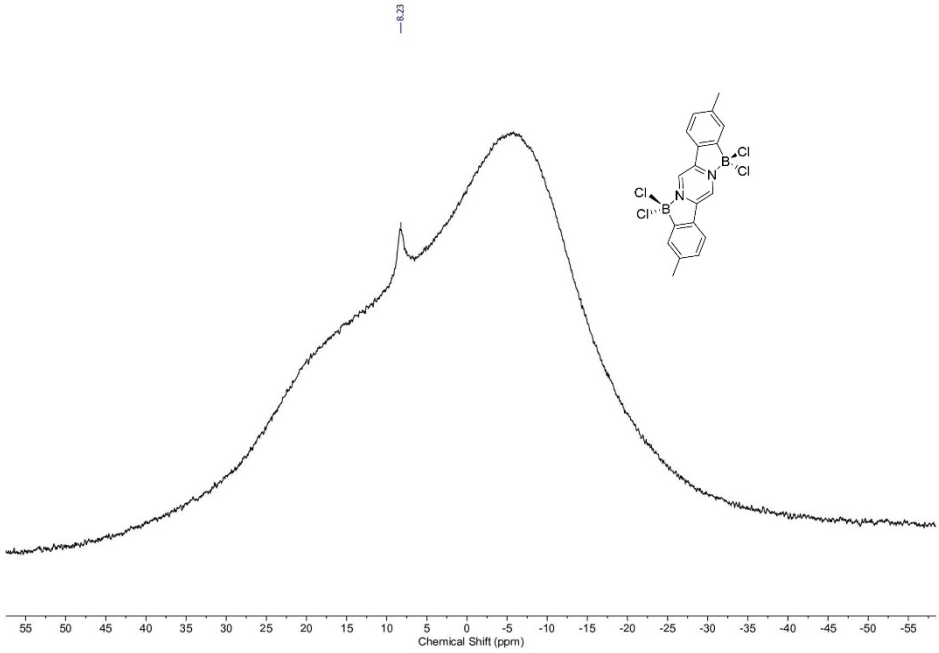

Figure S5. ^{11}B NMR of **BCl_2** in Acetone-d_6

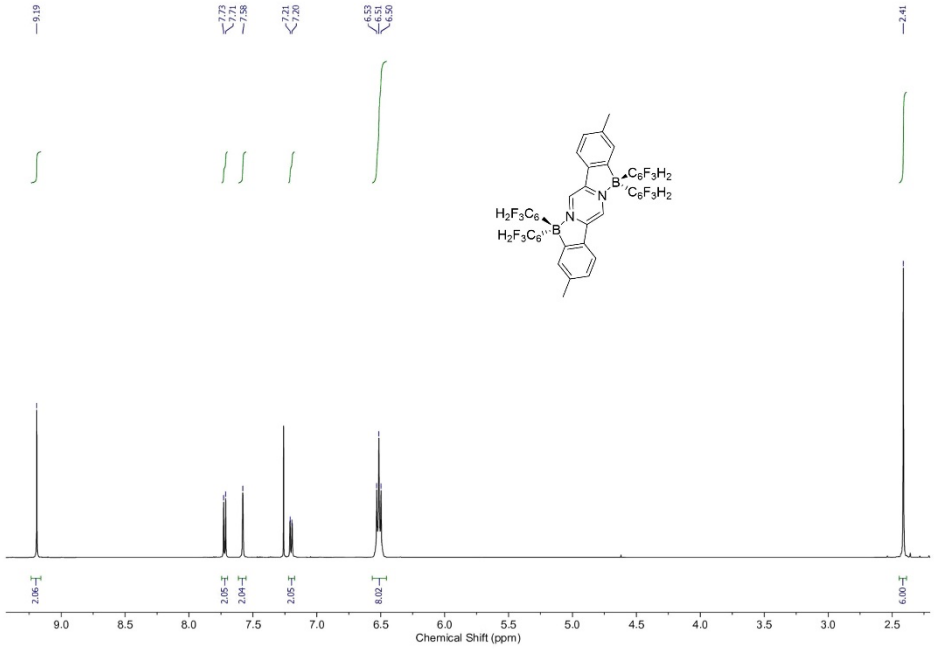

Figure S6. ^{1}H NMR of **1** in $CDCl_3$

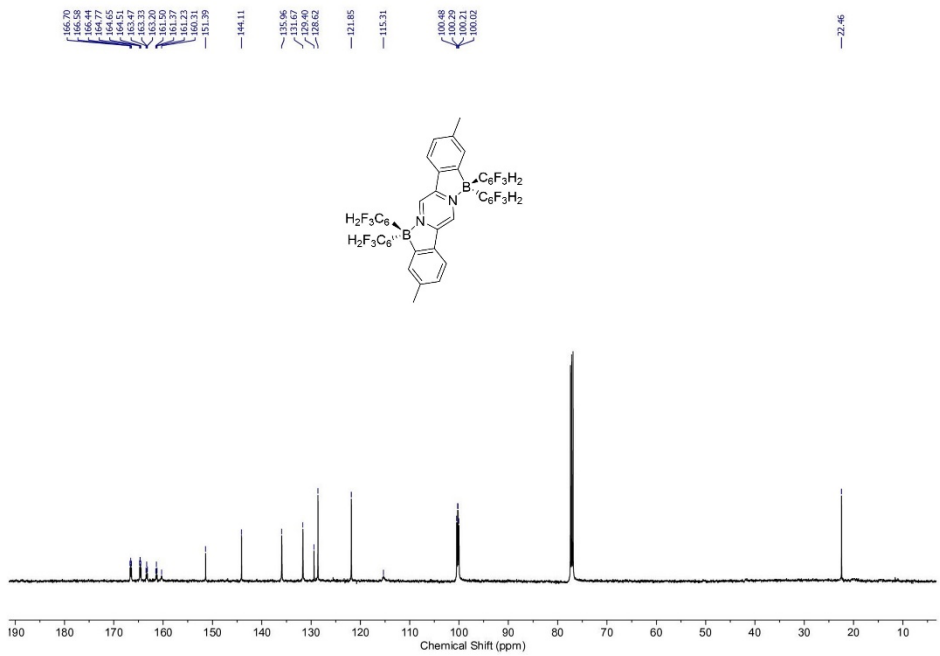

Figure S7. $^{13}C\ \{^{1}H\}$ NMR of **1** in $CDCl_3$

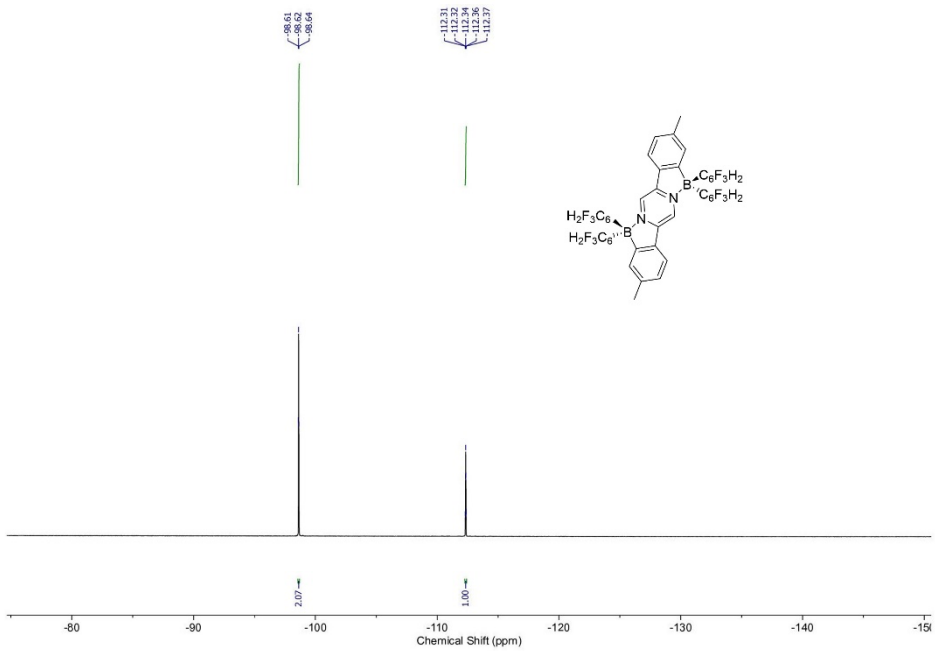

Figure S8. ^{19}F NMR of **1** in $CDCl_3$

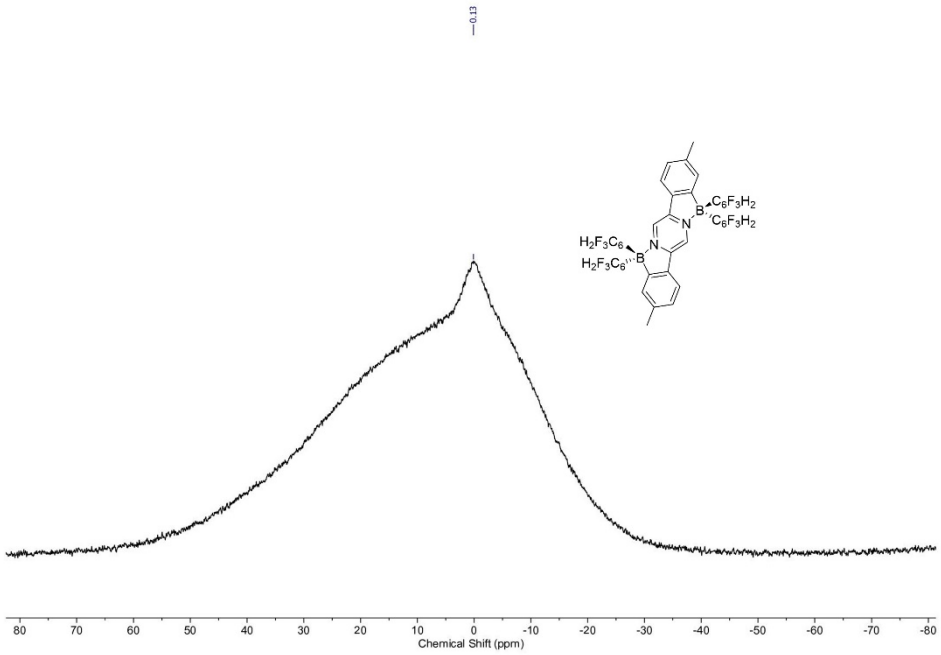

Figure S9. ^{11}B NMR of **1** in $CDCl_3$

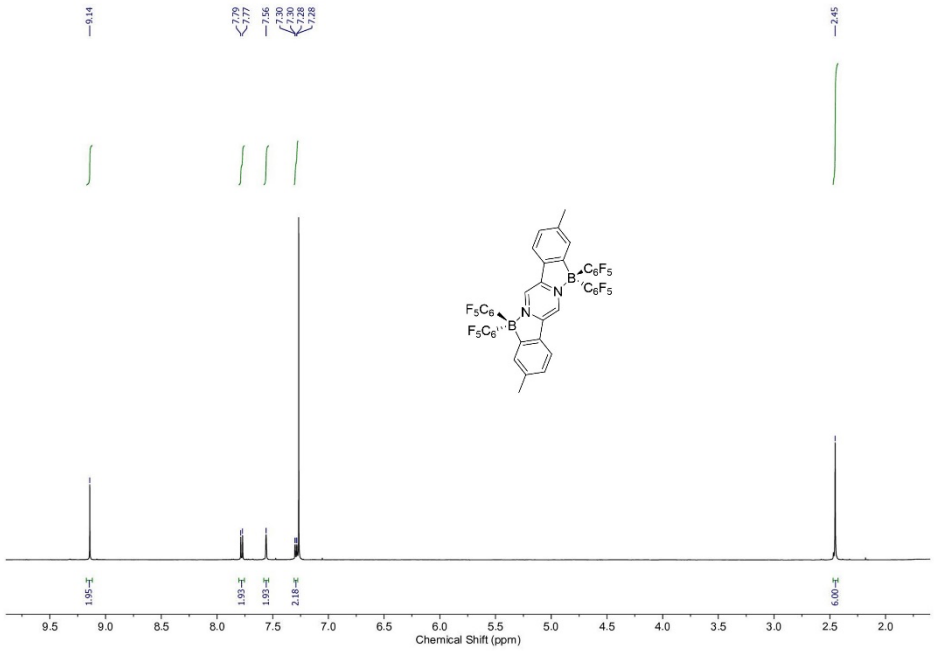

Figure S10. ^{1}H NMR of **2** in $CDCl_3$

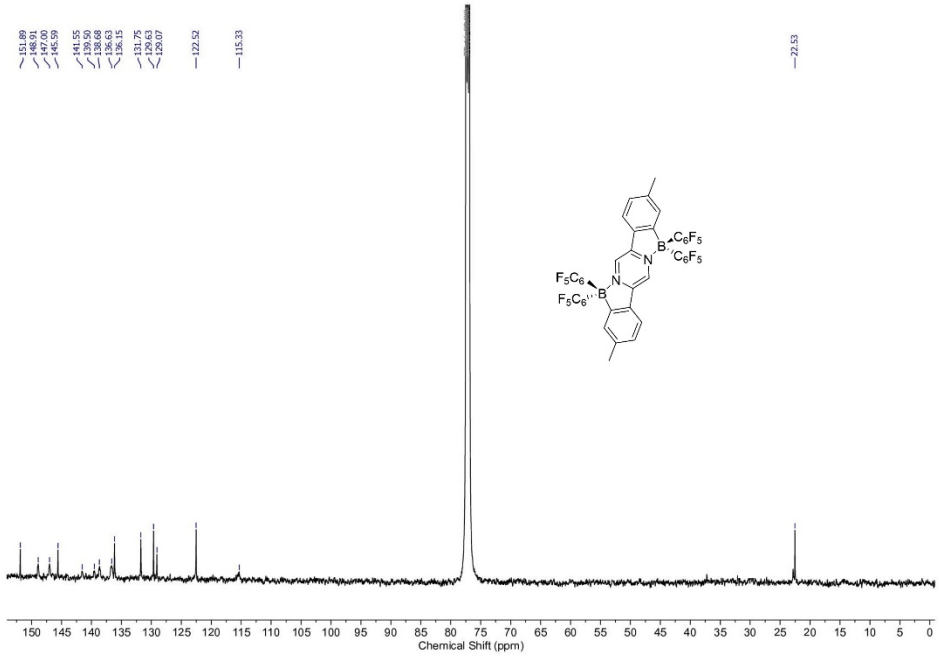

Figure S11. $^{13}C\ \{^{1}H\}$ NMR of **2** in $CDCl_3$

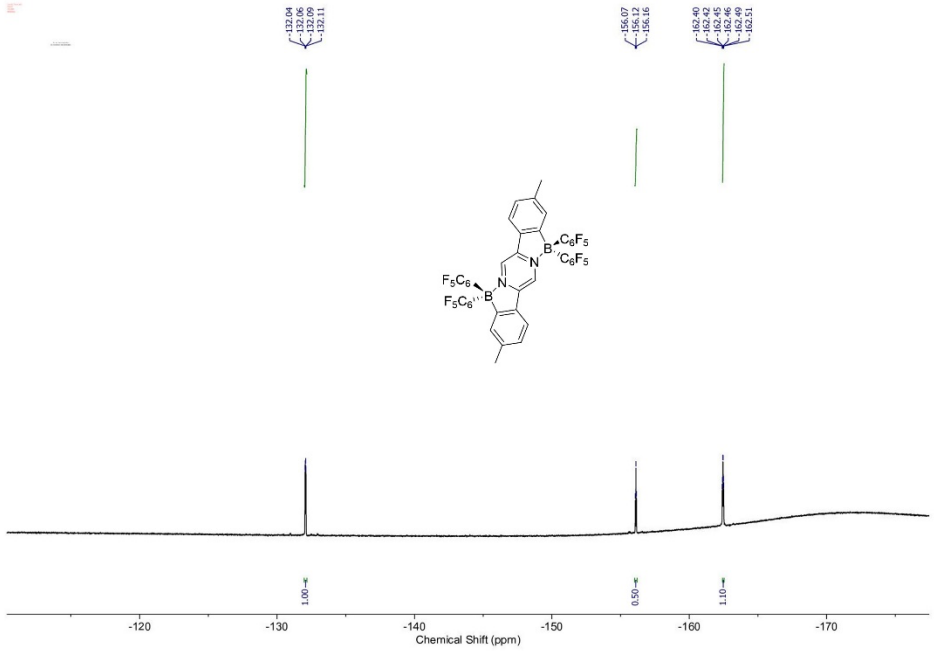

Figure S12. ^{19}F NMR of **2** in $CDCl_3$

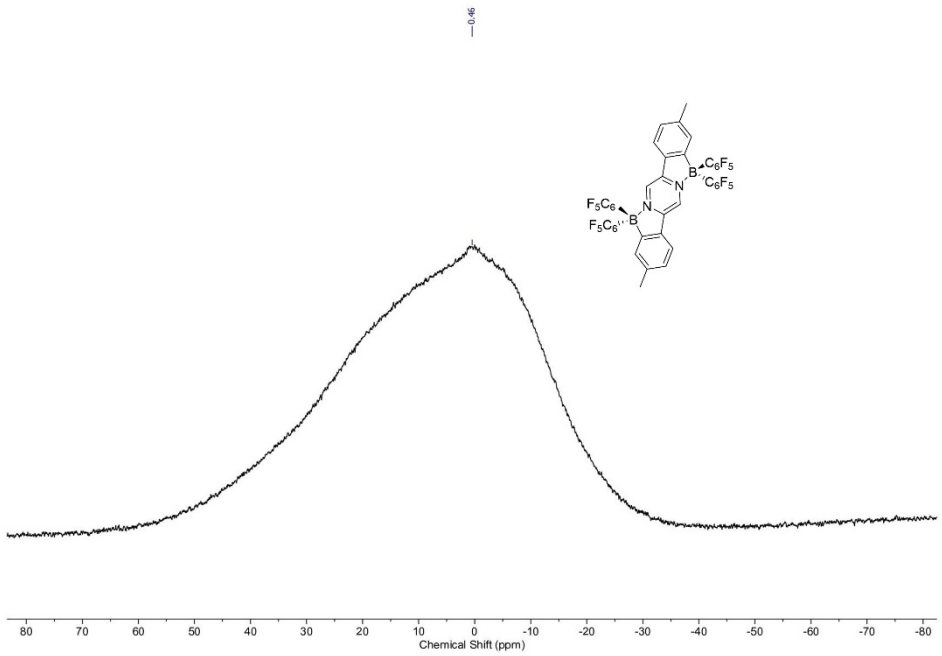

Figure S13. ^{11}B NMR of **2** in $CDCl_3$

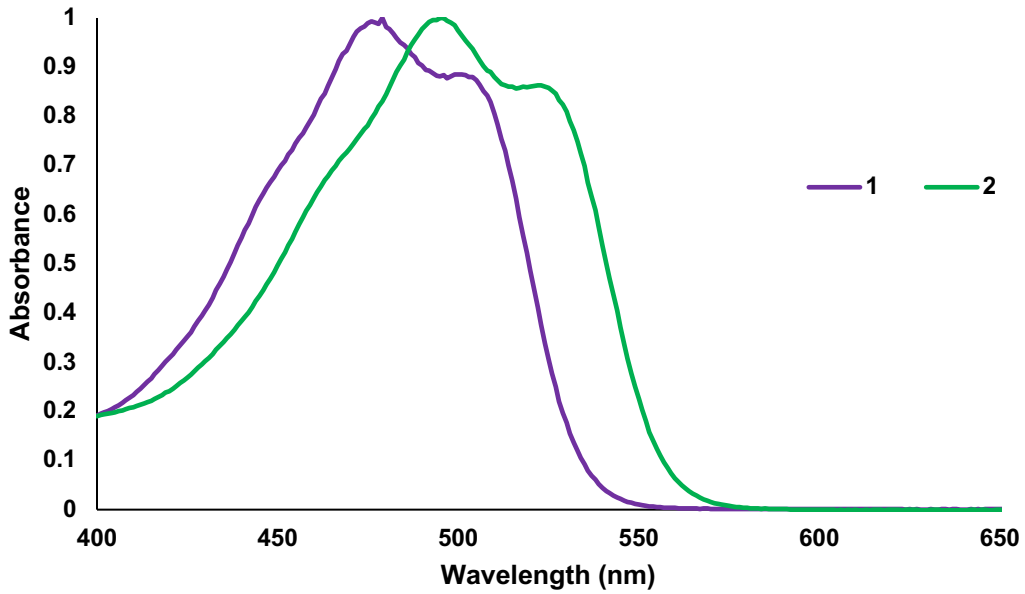

Figure S14. Normalized UV-Vis spectra of **1** and **2** recorded in 5×10^{-4} M CH_2Cl_2 solution.

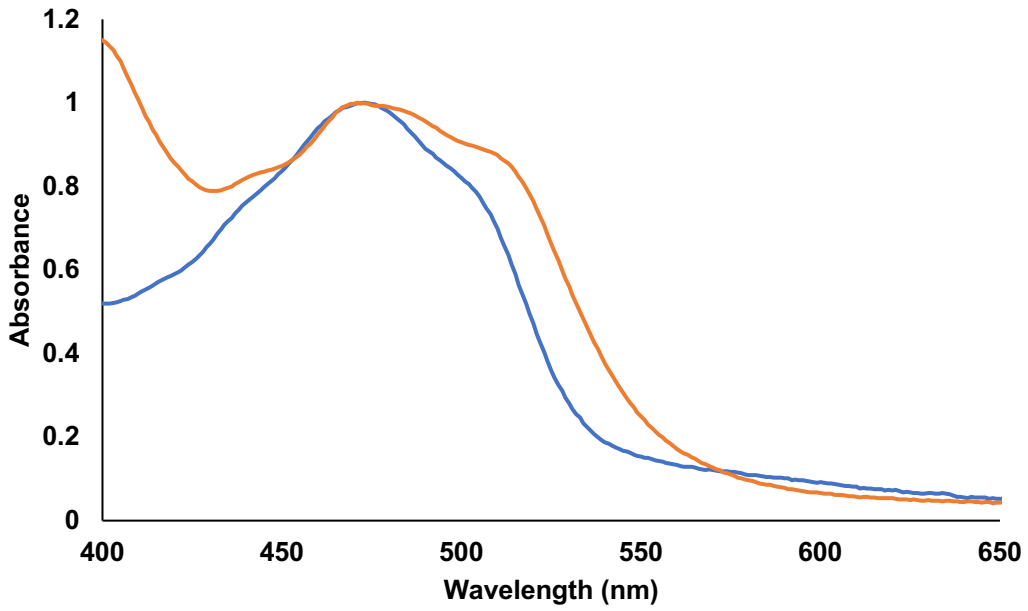

Figure S15. Normalized UV-Vis spectra of **1**$^{\bullet-}$ and **2**$^{\bullet-}$ recorded in 5×10^{-4} M CH_2Cl_2 solution.

Table S1. Crystal data and structure refinement for 2, $1^{\bullet-}$, and $2^{\bullet-}$.

Compound	**2** (CCDC 2127347)	$\mathbf{1}^{\bullet-}$ (CCDC 2127349)	$\mathbf{2}^{\bullet-}$ (CCDC 2127348)
Empirical formula	$C_{85}H_{30}B_4Cl_2F_{40}N_4$	$C_{62}H_{52}B_2CoF_{12}N_2$	$C_{52}H_{24}B_2CoF_{20}N_2$
Formula weight	1981.27	1133.60	1137.28
Temperature/K	173.0	173	173.0
Crystal system	triclinic	monoclinic	orthorhombic
Space group	P-1	$P2_1/n$	$Pna2_1$
a/Å	9.6307(2)	13.2272(14)	24.9525(12)
b/Å	15.9124(3)	14.4412(16)	11.0191(5)
c/Å	27.1357(5)	14.4045(16)	18.4802(7)
α/°	98.5650(10)	90	90
β/°	93.9640(10)	105.889(2)	90
γ/°	103.4580(10)	90	90
Volume/Å^3	3975.83(13)	2646.4(5)	5081.2(4)
Z	2	2	4
ρ_{calc}g/cm^3	1.655	1.423	1.487
μ/mm^{-1}	2.058	0.410	3.659
F(000)	1964.0	1166.0	2268.0
Crystal size/mm^3	0.322 × 0.202 × 0.048	0.351 × 0.198 × 0.064	0.232 × 0.222 × 0.089
Radiation	CuKα (λ = 1.54178)	MoKα (λ = 0.71073)	CuKα (λ = 1.54178)
2Θ range /°	3.312 − 140.11	4.074 to 56.602	7.084 to 133.198
Index ranges	$-11 \le h \le 11$, $-19 \le k \le 19$, $-33 \le l \le 33$	$-17 \le h \le 17$, $-19 \le k \le 19$, $-19 \le l \le 19$	$-29 \le h \le 25$, $-13 \le k \le 13$, $-22 \le l \le 21$
Reflections collected	56837	29164	32469
Independent reflections	14543 [R_{int} = 0.0313, R_{sigma} = 0.0375]	6579 [R_{int} = 0.0249, R_{sigma} = 0.0212]	8921 [R_{int} = 0.0395, R_{sigma} = 0.0353]
Data/restraints/parameters	14543/2932/1454	6579/0/366	8921/602/764
GooF	1.042	1.040	1.032
Final R indexes [I>=2σ (I)]	R_1 = 0.0574 wR_2 = 0.1595	R_1 = 0.0338, wR_2 = 0.0880	R_1 = 0.0520, wR_2 = 0.1393
Final R indexes [all data]	R_1 = 0.0644 wR_2 = 0.1664	R_1 = 0.0429, wR_2 = 0.0935	R_1 = 0.0662, wR_2 = 0.1496
Largest diff. peak/hole / e Å^{-3}	0.76/-0.64	0.32/-0.31	0.30/-0.27

References

(1) Sartori, P.; Weidenbruch, M. Darstellung Und Eigenschaften von. Pentafluorbenzoesäure-Derivaten. *Chem. Ber.* **1967**, *100* (9), 3016–3023. https://doi.org/10.1002/cber.19671000927.

(2) Stoll, S.; Schweiger, A. EasySpin, a Comprehensive Software Package for Spectral Simulation and Analysis in EPR. *J. Magn. Reson.* **2006**, *178* (1), 42–55. https://doi.org/10.1016/j.jmr.2005.08.013.

(3) Culham, S.; Lanoë, P.-H.; Whittle, V. L.; Durrant, M. C.; Williams, J. A. G.; Kozhevnikov, V. N. Highly Luminescent Dinuclear Platinum(II) Complexes Incorporating Bis-Cyclometallating Pyrazine-Based Ligands: A Versatile Approach to Efficient Red Phosphors. *Inorg. Chem.* **2013**, *52* (19), 10992–11003. https://doi.org/10.1021/ic401131x.

(4) Crossley, D. L.; Cid, J.; Curless, L. D.; Turner, M. L.; Ingleson, M. J. Facile Arylation of Four-Coordinate Boron Halides by Borenium Cation Mediated Boro-Desilylation and -Destannylation. *Organometallics* **2015**, *34* (24), 5767–5774. https://doi.org/10.1021/acs.organomet.5b00857.

(5) Morgan, M. M.; Nazari, M.; Pickl, T.; Rautiainen, J. M.; Tuononen, H. M.; Piers, W. E.; Welch, G. C.; Gelfand, B. S. Boron–Nitrogen Substituted Dihydroindeno[1,2- b]Fluorene Derivatives as Acceptors in Organic Solar Cells. *Chem. Comm.* **2019**, *55* (74), 11095–11098. https://doi.org/10.1039/C9CC05103A.